JCI insight

RESEARCH ARTICLE

MTH1 favors mesothelioma progression and mediates paracrine rescue of bystander endothelium from oxidative damage

Sophia F. Magkouta,[1] Apostolos G. Pappas,[1] Photene C. Vaitsi,[1] Panagiotis C. Agioutantis,[1] Ioannis S. Pateras,[2] Charalampos A. Moschos,[1] Marianthi P. Iliopoulou,[1] Chrysavgi N. Kosti,[1] Heleni V. Loutrari,[1] Vassilis G. Gorgoulis,[2,3,4] and Ioannis T. Kalomenidis[1]

[1]"Marianthi Simou Laboratory", 1st Department of Critical Care and Pulmonary Medicine, National and Kapodistrian University of Athens, School of Medicine, Evangelismos Hospital, Athens, Greece. [2]Molecular Carcinogenesis Group, Department of Histology and Embryology, School of Medicine, National Kapodistrian University of Athens, Athens, Greece. [3]Biomedical Research Foundation of the Academy of Athens, Athens, Greece. [4]Faculty of Biology, Medicine and Health, University of Manchester, Manchester Academic Health Science Centre, Manchester, United Kingdom.

Oxidative stress and inadequate redox homeostasis is crucial for tumor initiation and progression. MTH1 (NUDT1) enzyme prevents incorporation of oxidized dNTPs by sanitizing the deoxynucleoside triphosphate (dNTP) pool and is therefore vital for the survival of tumor cells. MTH1 inhibition has been found to inhibit the growth of several experimental tumors, but its role in mesothelioma progression remained elusive. Moreover, although MTH1 is nonessential to normal cells, its role in survival of host cells in tumor milieu, especially tumor endothelium, is unclear. We validated a clinically relevant MTH1 inhibitor (Karonudib) in mesothelioma treatment using human xenografts and syngeneic murine models. We show that MTH1 inhibition impedes mesothelioma progression and that inherent tumoral MTH1 levels are associated with a tumor's response. We also identified tumor endothelial cells as selective targets of Karonudib and propose a model of intercellular signaling among tumor cells and bystander tumor endothelium. We finally determined the major biological processes associated with elevated *MTH1* gene expression in human mesotheliomas.

Introduction

Oxidative stress from elevated reactive oxygen species (ROS) as well as insufficient redox regulation is a common phenotype of many cancers (1). Severe oxidative stress may lead to direct genotoxic damage and/or oxidation of the free deoxynucleoside triphosphate (dNTP) pool (2). Nevertheless, tumor cells adapt to such conditions by upregulation of the *MTH1 (NUDT1)* gene. This enzyme sanitizes their oxidized dNTP pools and, therefore, prevents incorporation of damaged nucleotides during DNA replication that would otherwise lead to DNA damage and cell death (3–6). MTH1 is, thus, crucial for tumor cell survival while it is nonessential for normal cells. This property makes it an appealing target for cancer therapy. Several MTH1 inhibitors have been designed and successfully tested in melanoma, colorectal, and breast cancer xenografts (3, 6–8). Karonudib (TH1579), the most potent inhibitor of the enzyme, is already under phase I clinical testing (Clinicaltrial.gov, NCT03036228).

Malignant pleural mesothelioma is the most common primary tumor of the pleural cavity, with an increasing global incidence (9). Currently, there is no effective treatment for mesothelioma. The vast majority of tumors are unresectable. The role of radiotherapy is limited, and chemotherapy (combinations of platinum and pemetrexed) offers only marginal survival benefit (10). Devising novel and effective therapies that can substantially curtail mesothelioma progression and significantly prolong survival remains an urgent and unmet need. Oxidative stress plays a central role in mesothelioma initiation and progression (11). Apart from mesothelioma cells, it is expected that other cells of tumor stroma, including endothelial cells, are also exposed to increased levels of oxidative stress (12, 13) and, therefore, may depend on MTH1 for their survival. We, thus, speculated that inhibition of MTH1 would prevent mesothelioma growth by targeting both tumor and tumor endothelial cells (TECs).

Our hypotheses were tested on 2 human mesothelioma xenograft and 2 murine syngeneic models using Karonudib (TH1579) as an MTH1 inhibitor. We have documented that MTH1 inhibition

Authorship note: AGP and PCV contributed equally to this work.

Conflict of interest: The authors have declared that no conflict of interest exists.

Submitted: November 8, 2019
Accepted: May 20, 2020
Published: June 18, 2020.

Reference information: *JCI Insight*. 2020;5(12):e134885. https://doi.org/10.1172/jci.insight.134885.

impedes mesothelioma progression and inherent tumoral MTH1 levels are associated with a tumor's response to MTH1 targeting. Importantly, we show that endothelial cells of the tumor niche are vulnerable to MTH1 inhibition and are selectively targeted by TH1579. We propose a model of intercellular signaling among tumor cells and bystander tumor endothelium. Finally, we present the transcriptome alterations in high versus low *MTH1*-expressing human mesotheliomas and their functional relation to biological processes, cellular components, and pathways.

Results

MTH1 promotes mesothelioma progression and can be pharmacologically targeted to impede mesothelioma in vivo. Survival analysis of mesothelioma patients revealed that high tumor *MTH1* mRNA expression was associated with a shorter survival (Figure 1A). We then investigated whether MTH1 inhibition would halt mesothelioma progression in vivo. To elucidate this, we first treated immunodeficient mice bearing ZL34 or MSTO-211H human mesothelioma tumors with TH1579 inhibitor (Karonudib). MTH1 inhibition substantially retarded human mesothelioma growth in both models (Figure 1, B and D). On the day of sacrifice, tumors of treated animals were 50% smaller (Figure 1, C and E) than respective ones of the control group. We subsequently expanded our observations to syngeneic mesothelioma models in order to study any potential effects of MTH1 inhibition in the tumor-host interactions. We therefore administrated the inhibitor to immunocompetent mice bearing AE17 or AB1 mesotheliomas. As seen in Figure 1, MTH1 inhibition significantly halted murine mesothelioma tumor growth (Figure 1F) and limited mesothelioma-associated pleural fluid accumulation (Figure 1G) in both models.

Karonudib efficiently targets MTH1 enzyme and elicits 8-Oxo-dG accumulation in mesothelioma tumors. MTH1 inhibition abrogates tumor cell proliferation, attenuates tumor-associated angiogenesis, and enhances tumor cell apoptosis in vivo. To corroborate the selectivity of Karonudib we measured the incorporation of 8-Oxo-dG lesions in tumor cell DNA. As seen in Figure 2, A and B, administration of the inhibitor conferred an increase of 8-Oxo-dG in all mesothelioma models. Phospho-histone H2AX29 (γH2AX), an established marker of DNA fragmentation due to apoptosis, was also increased in some cases (Supplemental Figure 2; supplemental material available online with this article; https://doi.org/10.1172/jci.insight.134885DS1). Having validated that the inhibitor had successfully abrogated MTH1, we subsequently evaluated its effects in tumor cell proliferation and apoptosis. Indeed, MTH1 inhibition led to reduced proliferation rates in all mesotheliomas (Figure 2, A and C) in vivo and mesothelioma cell viability in vitro (Supplemental Figure 1, A and B). Additionally, tumors of treated animals presented higher apoptosis rates compared with control ones in all mesothelioma models (Figure 2, A and D). Since DNA damage has been implicated in tumor-associated angiogenesis (14, 15), we investigated whether MTH1 inhibition affected neovascularization of the tumors. As shown in Figure 2E, tumors of TH1579-treated mice were less vascularized compared with vehicle-treated ones.

MTH1 levels are indicative of mesothelioma tumors' response to TH1579. While Karonudib provoked a 50% reduction of AB1 mesotheliomas (in accordance with the human xenographs), AE17 tumors were significantly — yet marginally — affected by the treatment (Figure 1F). We therefore questioned whether the 2 cell lines differ as for the expression of MTH1, the target of the inhibitor. Indeed, both AB1 cells and tumors exhibited significantly higher *Mth1* mRNA and protein levels compared with respective AE17 (Figure 3A). To validate the link between MTH1 expression levels and tumor sensitivity to TH1579, we overexpressed MTH1 (approximately 3 times) in the "less responsive" AE17 cells. Using an MTH1-expressing vector, we "silenced" MTH1 expression (approximately by 60%) into the "more responsive" AB1 cells (Supplemental Figure 3), and we repeated the in vivo experiments. As expected, silencing of MTH1 in AB1 cells retarded and overexpression of it in AE17 cells promoted mesothelioma growth (compared with vector cells) (Figure 3B) in vivo, although had no effect on cells' viability in vitro (data not shown). Most importantly, silencing of MTH1 rendered AB1 tumors unresponsive, while MTH1 overexpression significantly sensitized AE17 mesotheliomas to the inhibitor (Figure 3C). The aforementioned in vivo observations were in accordance with the 8-Oxo-dG accumulation pattern of all groups in both models (Figure 3, D and E).

Tumor endothelium overexpresses MTH1 and is selectively targeted by Karonudib, unlike the normal one. As previously mentioned, tumor cell dependency on MTH1 lies on the dysfunctional redox regulation and elevated ROS of the tumor microenvironment. We assumed that coping with oxidative stress and genotoxic damage should also be important for the survival of all host cells residing the tumor microniche. Having shown that

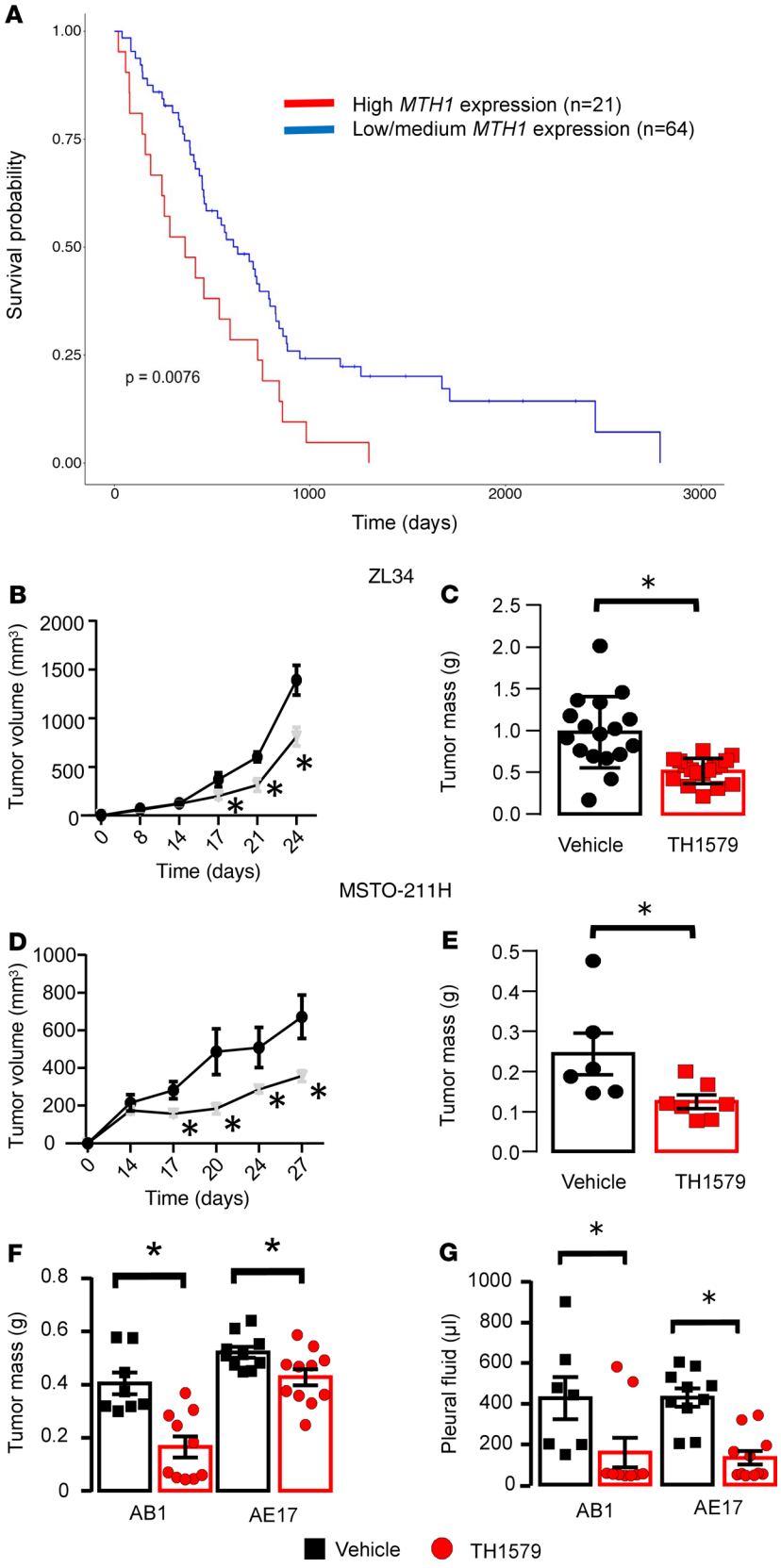

Figure 1. High *MTH1* (*NUDT1*) mRNA is associated with shorter patient survival. MTH1 inhibition retards mesothelioma progression in vivo. (**A**) RSEM data of RNA-seq analysis retrieved by the TCGA biobank were analyzed using the UALCAN portal. Kaplan-Meier plot correlating *NUDT1* gene expression with mesothelioma patients' survival (high *MTH1*, $n = 21$; low/medium *MTH1*, $n = 64$). *P* value was obtained upon log-rank test. (**B–E**) Human mesothelioma tumors were created upon s.c. injection of 2×10^6 ZL34 or MSTO-211H cells in NOD.SCID mice. TH1579 administration commenced once tumors became 200 mm^3. Mice received vehicle or TH1579 (90 mg/kg body weight) 2 times per day, every 2 days. Tumor size was measured by a digital caliper (**B** and **D**). On the day of sacrifice, mesothelioma tumors were excised and weighed (**C** and **E**). Data presented as mean ± SEM. ZL34: vehicle and TH1579, $n = 17$ mice each. MSTO-211: vehicle, $n = 6$ mice; TH1579, $n = 7$ mice. $^*P < 0.05$ compared with vehicle by 2-tailed Students' *t* test. (**F** and **G**) AB1 and AE17 cells were intrapleurally injected into syngeneic BALB/c and C57BL/6 mice, respectively, and animals were treated as above. Fourteen days later, mice were sacrificed and mesothelioma tumors were excised and weighed (**F**) and pleural fluid was retrieved and quantified (**G**). Data presented as mean ± SEM. AB1: vehicle, $n = 8$ mice; TH1579, $n = 10$ mice. AE17: vehicle, $n = 10$ mice; TH1579, $n = 11$ mice. $^*P < 0.05$ compared with vehicle by 2-tailed Students' *t* test.

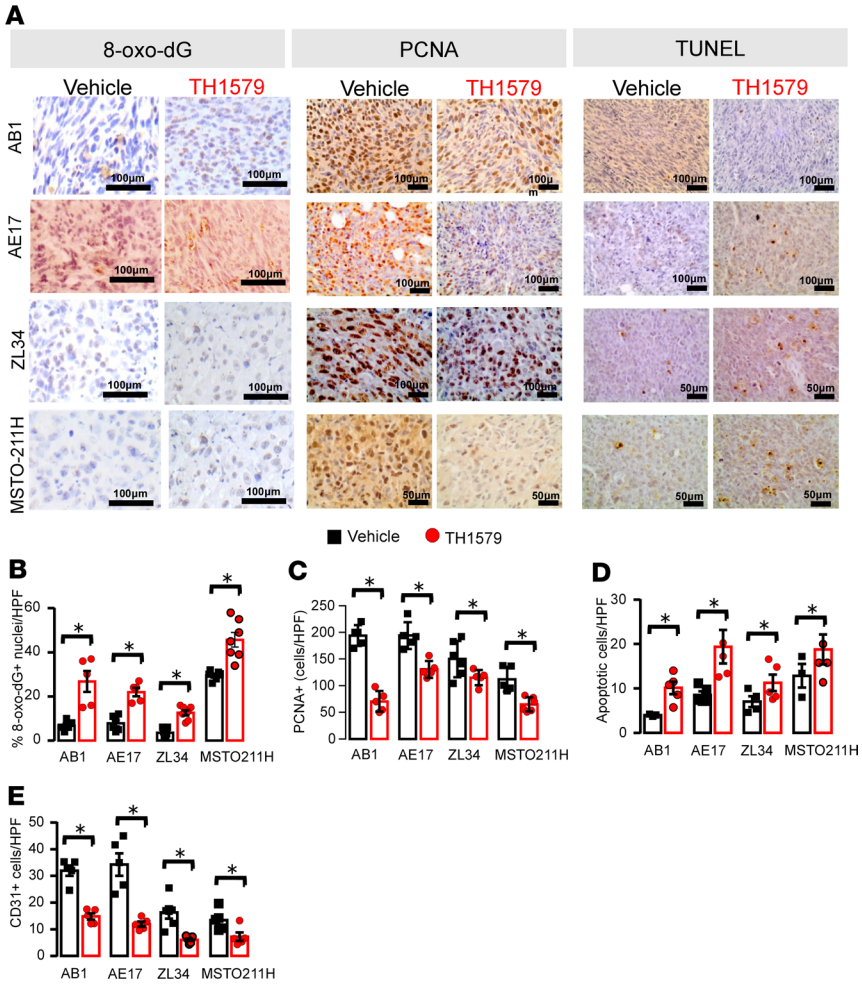

Figure 2. MTH1 inhibition elevates tumor cell 8-Oxo-dG levels in mesothelioma tumor cells, reduces tumor cell proliferation and tumor angiogenesis, and enhances tumor cell apoptosis in experimental mesotheliomas. (**A–E**) Tumor tissue sections were stained for 8-Oxo-dG lesions in order to validate MTH1 inhibition in TH1579-treated animals (**A** and **B**). Tumor cell proliferation rates were also determined upon PCNA staining (**A** and **C**), while tumor cell apoptosis was evaluated using the TUNEL assay (**A** and **D**). Angiogenic density of all tumors was also determined upon CD31 staining (**E**). Data presented as mean ± SEM. AB1: vehicle, $n = 5$; TH1579, $n = 5$. AE17: vehicle, $n = 6$; TH1579, $n = 5$. ZL34: vehicle, $n = 5$; TH1579, $n = 7$. MSTO-211: vehicle, $n = 5$; TH1579, $n = 7$. $^*P < 0.05$ compared with vehicle by 2-tailed Students' t test. HPF, high power field.

MTH1 inhibition limits tumor angiogenesis (Figure 1E), we focused on TECs, which are known to have acquired resistance to ROS (12). We compared *Mth1* mRNA levels of freshly isolated TECs and normal ones. TECs have elevated *Mth1* mRNA levels compared with adjacent normal endothelial cells (NECs), and *Mth1* expression is higher in TECs from high-MTH1–expressing tumors than those from the low-expressing ones (Figure 4A). Tumor endothelium could, thus, be vulnerable to MTH1 inhibition. We therefore analyzed apoptosis of TECs by dual staining of CD31 and caspase-3 in mesothelioma specimens. Tumors from Karonudib-administered animals exhibited higher levels of apoptotic endothelial cells (Figure 4B), implying enhanced vessel regression rather than reduced neovascularization. Accordingly, high TEC MTH1 expression was associated with less baseline apoptotic endothelial cells and more pronounced AE17 TH1579–induced TEC apoptosis (Figure 4B). TECs were also shown to be sensitive to Karonudib treatment in vitro, while NECs remain unaffected (Figure 4C). We further expanded these observations by investigating whether key angiogenic properties of TECs are selectively affected compared with NECs. Indeed, TH1579 successfully impaired TEC migration (Figure 4D) and de novo tube formation (Figure 4E), while it did not affect NECs. Intriguingly, TECs isolated from AE17 MTH1–overexpressing tumors were more sensitive to TH1579 effects compared with TECs isolated from AE17 tumors (Figure 4, C–E). Overall, the above observations suggest

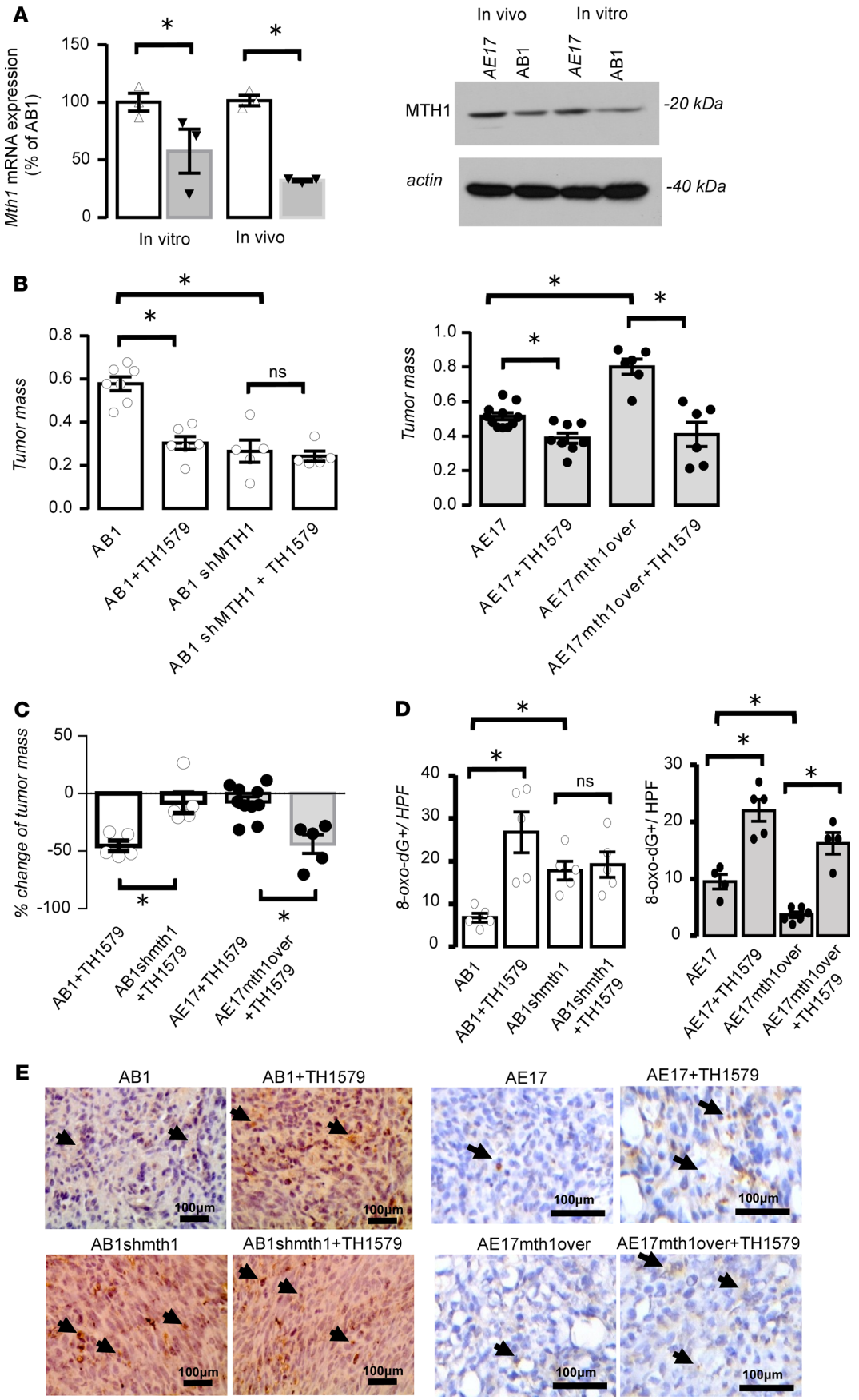

Figure 3. Tumors' response to Karonudib is associated with intrinsic MTH1 expression levels. (**A**) *Mth1* mRNA (left) and protein (right) expression levels of murine mesothelioma cells and tumors were determined by real-time PCR and Western blotting, respectively. Data presented as mean ± SEM, $n = 3$ for each group,$^*P < 0.05$ compared with AB1 by 2-tailed Students' t test. (**B**) AB1 cells silenced for MTH1 expression (AB1shmth1) and respective AB1 vector cells (left), or AE17 MTH1–overexpressing cells and respective AE17 vector cells (right), were intrapleurally injected into syngeneic mice and treated as aforementioned. Fourteen days later, mice were sacrificed and mesothelioma tumors were excised and weighed. Data presented as mean ± SEM. AB1, $n = 7$; AB1+TH1579, $n = 6$; AB1shmth1, $n = 5$; AB1shmth1+th1579, $n = 5$; AE17, $n = 11$; AE17+TH1579, $n = 8$; AE17 MTH1–overexpressing (AE17mth1over), $n = 7$; AE17mth1over+TH1579, $n = 6$. $^*P < 0.05$ for indicated comparisons by 1-way ANOVA (with Bonferroni's post hoc test). (**C**) Tumor's response to TH1579 inhibitor was evaluated as percent of change of tumor weight referred to respective control group by 2-tailed Students' t test. Data presented as mean ± SEM, n as in **B**.$^*P < 0.05$ compared with indicated comparisons. (**D** and **E**) Tumor sections of all groups were analyzed for 8-Oxo-dG expression. Data presented as mean ± SEM. AB1, $n = 5$ for each group; AE17, $n = 5$ for AE17, AE17+TH157, and AE17mth1over+TH1579 groups; AE17mth1over, $n = 7$ each. $^*P < 0.05$ compared with indicated comparisons by 1-way ANOVA (with Bonferroni's post hoc test). (**E**) Representative pictures of tumor tissue sections stained for 8-Oxo-dG (black arrows). HPF, high power field. Scale bar: 100 μm. Arrows depict positive nuclear staining.

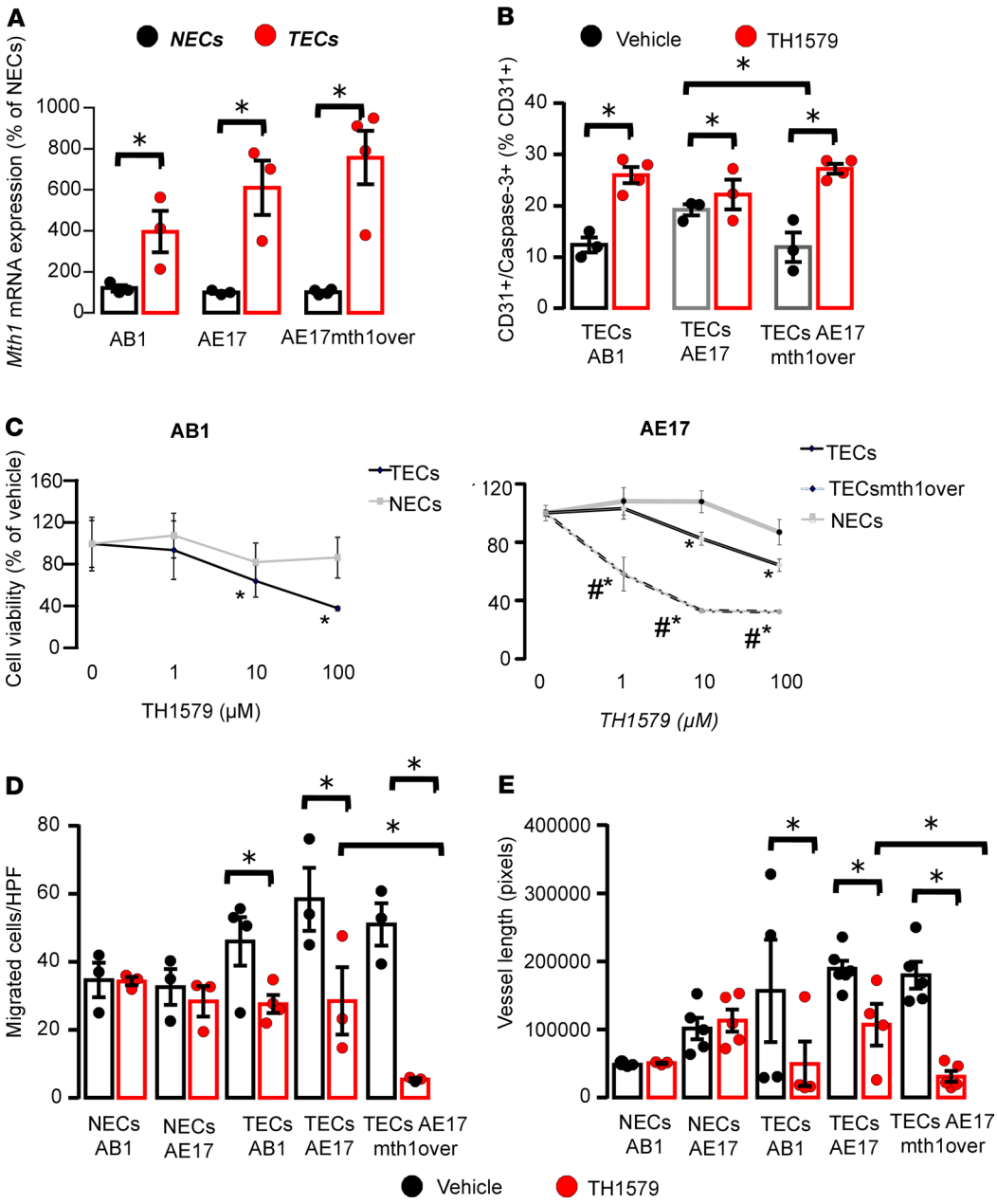

Figure 4. MTH1 is overexpressed by tumor endothelium, and tumor endothelial cells are selectively targeted by Karonudib. Endothelial cells of MTH1-overexpressing tumors are more sensitive to MTH1 inhibition. (**A**) Endothelial cells from AB1, AE17, and AE17 MTH1–overexpressing tumors (TECs) and normal endothelial cells (NECs) from lung tissue were isolated, and mRNA levels of *Mth1* was quantified by real-time PCR. Data are presented as mean ± SEM, n = 3 for each group. *P < 0.05 compared with NECs by 2-tailed Students' t test. (**B**) Endothelial cells of AB1, AE17, and AE17 MTH1–overexpressing tumors from mice treated with vehicle or TH1579 were isolated using magnetic beads bearing anti-CD31 antibody. TECs were fixed, permeabilized, and stained for caspase-3 in order to measure apoptotic cells using flow cytometry. Data are presented as mean ± SEM, n = 3 for each vehicle and n = 4 for each TH1579 group. *P < 0.05 compared with indicated groups by 2-tailed Students' t test. (**C**) Isolated TECs and NECs from AB1, AE17, and AE17 MTH1–overexpressing mesotheliomas were seeded at 6 × 10^3 cells/well in 96-well plates and subsequently treated with escalating doses of TH1579 (1–1000 μM). Cell viability was determined by XTT reduction. Data are presented as mean ± SEM, n = 6 for each group. *P < 0.05 compared with vehicle by 2-tailed Students' t test. #P < 0.05 compared with TECs by 2-tailed Students' t test. (**D**) Alternatively, the aforementioned isolated TECs and NECs were serum starved for 4 hours and challenged to migrate toward full medium. Data are presented as mean ± SEM. n = 3 for both groups of AB1 and AE17 NECs, AE17 TECs, AE17 MTH1–overexpressing (AE17mth1over) TECs; n = 4 for each group of AB1 TECs. *P < 0.05 compared with indicated groups by 2-tailed Students' t test. (**E**) The aforementioned isolated TECs and NECs were challenged to form capillary-like tubes de novo on Matrigel. Data are presented as mean ± SEM, n = 3 for both groups of AB1 NECs, n = 5 for both groups of AE17 NEC and AE17mth1over TECs, n = 4 for each group of AB1 and AE17 TECs. *P < 0.05 compared with indicated groups by 2-tailed Students' t test.

that tumor endothelium overexpresses MTH1 and it is selectively targeted by the MTH1 inhibitor. Additionally, endothelial MTH1 expression follows the pattern of the tumor MTH1 expression.

Tumor cell actively supports TECs' survival of oxidative stress by upregulating their MTH1. Having witnessed an association of tumor cell MTH1 levels with endothelial ones, we subsequently focused on revealing the mechanistic basis underlying this observation. We assumed that differences in MTH1 levels of the tumor cells would mainly affect the oxidized DNA and/or the extracellular dNTP pool and that tumor cell DNA might serve as a paracrine signal that regulates TEC MTH1 expression and survival. We therefore isolated DNA from AE17 MTH1–overexpressing tumor cell supernatants and analyzed them using a Bioanalyzer. Evaluation of the sizes of DNA isolated revealed high–molecular weight genomic DNA (Figure 5A), implying that it is a result of active cellular secretion commonly mediated by microvesicles (16–18). We subsequently evaluated the oxidation levels of the DNA secreted by the high and low MTH1 tumor cells by determining their 8-Oxo-dG content. As expected, DNA isolated from AE17 cell supernatants had significantly higher levels of 8-Oxo-dG compared with DNA collected from supernatants of AE17 cells overexpressing MTH1 (Figure 5B). Interestingly, treatment of AE17 cells with the antioxidant N-acetyl cysteine limited 8-Oxo-dG incorporation at DNA secreted by AE17 cells (Figure 5B).

Since dsDNA can be detected by TLR9 receptors (19), we subsequently hypothesized that DNA secreted by tumor cells could trigger the TLR9/NF-κB axis in bystander TECs. Indeed, DNA secreted by AE17 cells enhanced NF-κB p65 phosphorylation/activation in TECs (Figure 5C). Most importantly, TLR9/NF-κB activation of endothelial cells is critically affected by the oxidation level of the secreted tumor DNA. The more oxidized DNA secreted by AE17 cells provoked a significant activation of NF-κB in TECs compared with that excreted by MTH1-overexpressing AE17 cells or by AE17 cells treated with antioxidant (Figure 5D). This effect was (at least partially) reversed by the TLR9 inhibitor (Figure 5D).

We subsequently evaluated the impact of differentially oxidated tumor cell-free DNA (cfDNA) on MTH1 levels and survival of TECs. Treatment of TECs with cfDNA derived from MTH1-overexpressing tumor cells significantly upregulated the MTH1 of TECs (Figure 5E) and enhanced their survival (Figure 5G). To test whether this effect is NF-κB mediated, we exposed TECs to cfDNA from control AE17, AE17 MTH1–overexpressing cells, and control AE17 treated with antioxidant and examined their effects on interaction between NF-κB and the *MTH1* promoter in TECs. Highly oxidized DNA from AE17 cells significantly enhanced NF-κB interactions with the *Mth1* gene (Figure 5F). In line with these observations, NF-κB negatively regulates the *Mth1* gene in endothelial cells. Treatment of TECs with TNF-α or PMA (2 well characterized NF-κB inducers) downregulated their MTH1 expression (Supplemental Figure 4). In accordance with this, inhibition of NF-κB reversed the effects of secreted DNAs on TEC MTH1 (Supplemental Figure 4). Collectively, tumor cells of high intrinsic MTH1 levels secrete DNA of low oxidation state that suppresses NF-κB activation in TECs, leading to upregulation of their MTH1 levels and favoring their survival.

MTH1 expression in human mesotheliomas is associated with genes involved in cell cycle and the microvesicle trafficking. In order to obtain deeper biological insights on the role of MTH1 expression in mesothelioma progression, we evaluated the available TCGA RNA sequencing (RNA-seq) data of mesothelioma patients to unveil differentially expressed genes (DEGs) and major relevant biological processes and pathways involved. More specifically, we selected patients whose tumor *NUDT1* (*MTH1*) expression was above the 75% percentile and those below the 25% percentile (14 patients per group) (Figure 6A). Our analysis revealed a total of 279 DEGs between high and low *MTH1*-expressing mesotheliomas, 135 of which were upregulated and 144 were downregulated in the former group (Figure 6B and Supplemental Table 1). Gene ontology (GO) analysis of DEGs revealed a statistically significant relation, with a total of 78 biological processes that are mainly associated with cell cycle/mitosis, cytoskeleton reorganization, and DNA repair (Figure 6C). Noteworthy, apart from the anticipated implication of *MTH1* in the aforementioned processes, our analysis revealed a significant association of *MTH1* with terms related to the microvesicle transport system (GO terms assigned as vesicle coating, nucleocytoplasmic transport, endomembrane system organization, COPII-coated vesicle cargo loading, vesicle targeting [to, from, or within Golgi], or Golgi vesicle budding) (Figure 6C and Supplemental Table 2). Furthermore GO analysis of cellular components unveiling the subcellular location of relevant actions (Figure 6D and Supplemental Table 3), as well as Reactome Pathway analysis outlining the involved molecular pathways (Figure 6E and Supplemental Table 4), also corroborated with a role of MTH1 in microvesicle trafficking, as indicated by relevant terms (tethering complex, COPII vesicle coat, vesicle coat). Noteworthy, DEG analysis revealed many genes (*RAB3GAP2*, *RAB33*, *RABAC1*, *ATF2*, *ATF6*, *TREX1*, *PTP14N*, *ERN1*, *GADD45GIP1*) that are currently associated with DNA damage–associated ER stress (20–22).

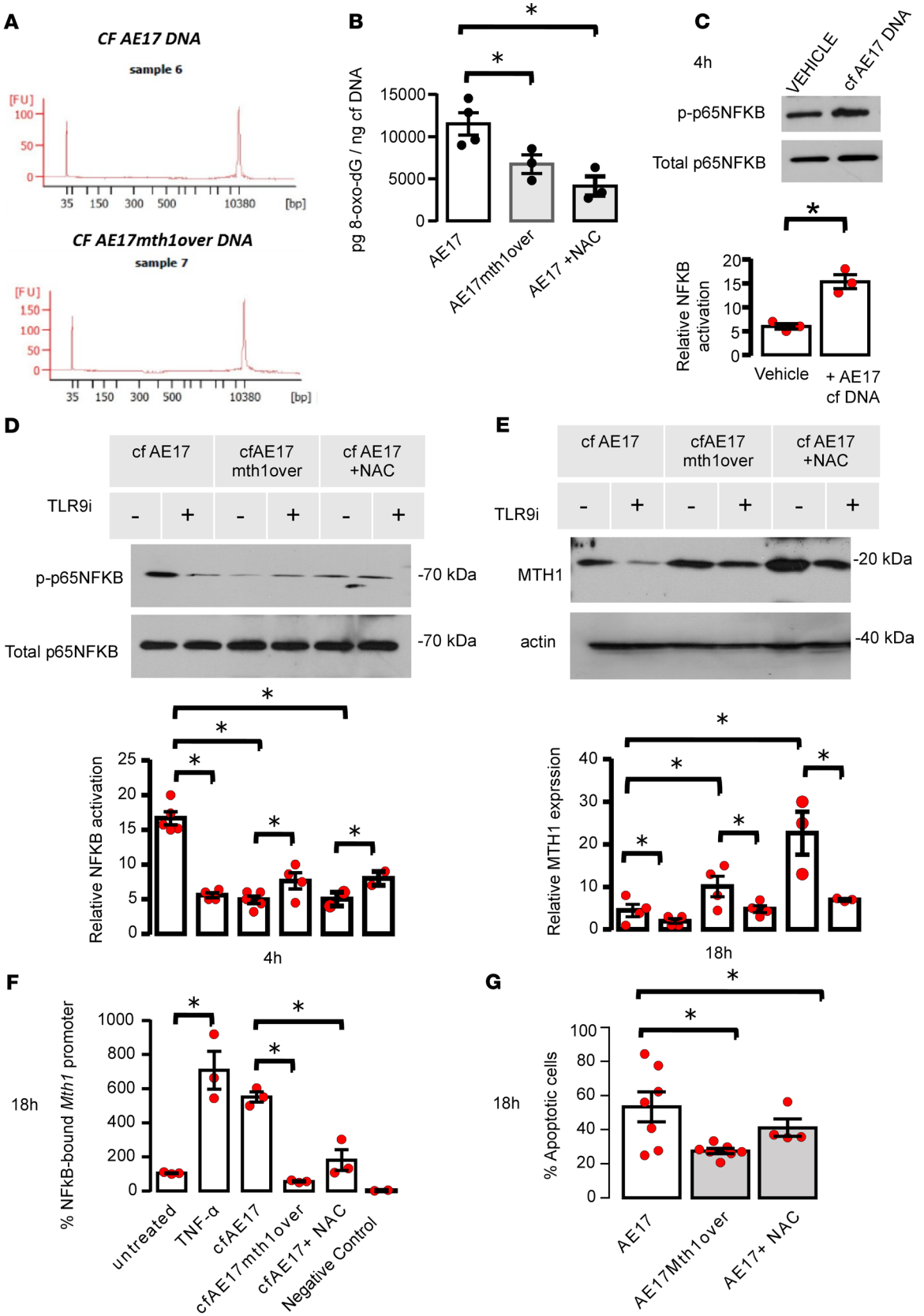
A
CF AE17 DNA
sample 6
[FU]
100
50
0
35 150 300 500 10380 [bp]
CF AE17mth1over DNA
sample 7
[FU]
150
100
50
0
35 150 300 500 10380 [bp]
B
pg 8-oxo-dG / ng cf DNA
15000
10000
5000
0
AE17
AE17mth1over
AE17 +NAC
C
4h
VEHICLE
cf AE17 DNA
p-p65NFKB
Total p65NFKB
Relative NFKB activation
20
15
10
5
0
Vehicle
+ AE17 cf DNA
D
cf AE17
cfAE17 mth1over
cf AE17 +NAC
TLR9i
- + - + - +
p-p65NFKB
-70 kDa
Total p65NFKB
-70 kDa
Relative NFKB activation
25
20
15
10
5
0
4h
E
cf AE17
cfAE17 mth1over
cf AE17 +NAC
TLR9i
- + - + - +
MTH1
-20 kDa
actin
-40 kDa
Relative MTH1 exprssion
40
30
20
10
0
18h
F
18h
% NFkB-bound Mth1 promoter
1000
800
600
400
200
0
untreated
TNF-α
cfAE17
cfAE17mth1over
cfAE17+ NAC
Negative Control
G
18h
% Apoptotic cells
100
80
60
40
20
0
AE17
AE17Mth1over
AE17+ NAC

Figure 5. cfDNA of MTH1-overexpressing tumors upregulates MTH1 expression of tumor endothelial cells through TLR9/NF-κB axis and promotes their survival. (**A**) AE17 and AE17 MTH1–overexpressing cells secrete large genomic DNA fragments. Nucleic acid isolated from AE17 and AE17 MTH1–overexpressing (AE17mth1over) cell culture supernatants were analyzed by capillary electrophoresis. Representative electropherograms of AE17 (top) and AE17mth1overexpressing cell (bottom) nucleic acids. (**B**) Oxidative state of cfDNA secreted by AE17 tumor cells is higher than that of AE17 mth1–overexpressing cells. Addition of antioxidant can prevent 8-Oxo-dG incorporation into DNA. cfDNA isolated from cell culture supernatants of AE17 (n = 4), AE17mth1over (n = 3), or AE17 cells treated with NAC (5 mM, overnight) (n = 3) was analyzed for the presence of 8-Oxo-dG by ELISA. Results were normalized to total DNA (ng). (**C**) cfDNA secreted by AE17 cells activates NF-κB in TECs. Serum-starved TECs were treated with vehicle or cfDNA from AE17 for 4 hours. Phosphorylated and total p65–NF-κB was detected by Western blot. (**D**) "More oxidized" cfDNA triggers a higher NF-κB activation than "less oxidized" cfDNA, through TLR9. Serum-starved TECs were treated with TLR9i (2 μg/mL) or vehicle for 40 minutes and subsequently treated with 20 ng/mL cfDNA from AE17, AE17 MTH1–overexpressing cells, or AE17 cells treated with NAC for 4 hours. Phosphorylated and total p65–NF-κB was measured by Western blot. (**E**) cfDNA of MTH1-overexpressing tumor cells upregulates MTH1 of TECs through TLR9. TECs were treated as described in **D** and analyzed for MTH1 expression by Western blot. (**F**) NF-κB binds to the endogenous MTH1 promoter of TECs. TECs were treated as **C** (n = 3). TNF-α (20 ng/mL) was used as a positive control. Binding of NF-κB to MTH1 gene promoter was determined by ChIP assay and Real-time PCR. Results were normalized to the input DNA control. A negative control (NC) (no antibody) was included. (**G**) TECs were treated as in **C**, and apoptotic cells were determined upon annexin V–PI staining (AE17, n = 7; AE17mth1over, n = 7; AE17+NAC, n = 4). (**C–E**) One representative blot of 3 independent experiments. All data are presented as the mean ± SEM. (**B**, **F**, **G**) *P < 0.05 compared with indicated groups by 1-way ANOVA (with Bonferroni's post hoc test for multiple comparisons). (**C**, **D**, **E**) *P < 0.05 compared with indicated groups by 2-tailed Students' t test.

Intriguingly, a single GO term associated with vascular development (Supplemental Table 2) was retrieved by our analysis, but apart from *KDR* (gene encoding for VEGFR2) no other classical angiogenic signature genes seemed to be involved. Noteworthy, among the upregulated genes, *TREX1* and *GPX1* (Supplemental Table 1) have been recently shown to enhance tumor angiogenesis mainly by reinforcing endothelial cell oxidative defense and subsequent survival and sprouting (12, 23). The aforementioned results, while they cannot safely rule out the implication of one of the classical angiogenic pathways, do argue toward the notion that MTH1 and DNA repair provide an alternative route of tumor angiogenesis.

Discussion

We here investigated the effect of MTH1 inhibition in malignant mesothelioma. Our main findings are: (a) elevated tumor *NUDT1* mRNA levels are associated with short patients' survival; (b) pharmacological targeting of MTH1 limited mesothelioma progression in vivo and hindered mesothelioma-associated pleural fluid accumulation, and impaired MTH1 activity favored the formation of oxidative 8-Oxo-dG DNA lesions, attenuated tumor cell proliferation and tumor-associated angiogenesis, and promoted tumor cell apoptosis in vivo; (c) intrinsic levels of MTH1 are associated with tumor cell sensitivity to MTH1 inhibitor; (d) TECs overexpress MTH1 and are therefore selectively targeted by the inhibitor, which induces apoptosis of TECs in vivo, abrogate survival, migration, and tube formation in vitro; (e) Tumor cells promote survival of TECs, upregulating their MTH1 through the DNA fragment–induced, TLR9-mediated NF-κB axis; and (f) MTH1 expression in human mesothelioma tumors significantly associates with DNA repair, mitosis, actin reorganization, and ER stress vesicle formation and trafficking.

This is the first study to our knowledge that explores the effect of an already clinically tested MTH1 inhibitor Karonudib (TH1579) in mesothelioma models. The most interesting property of this class of anticancer agents is that it selectively targets tumor cells, while it is well tolerated by the host (3, 6). In addition, since their antitumor effects are not dependent on specific tumor mutational status, they pledge to overcome problems arising from intratumor heterogeneity and acquisition of resistance. Relative to this, a recent study in melanoma presented that effectiveness of TH1579 was independent of the presence of the most common melanoma-driver genes (7). An additional property of superior clinical importance is that MTH1 inhibitors are expected to overcome the severe toxicity issues often raised by current anticancer agents. In our hands, TH1579 was found to impede mesothelioma progression, affecting tumor cell proliferation and survival. The observed effects coincided with an enhanced incorporation of 8-Oxo-dG lesions to tumor cell DNA and come in accordance with previous studies (6, 24). Interestingly, although overexpression of MTH1 in tumor cells has been reported to rescue them from TH1579 treatment in vitro (6), we here demonstrate that overexpression of MTH1 sensitized AE17 mesothelioma tumors to MTH1-targeting therapy in vivo. Similarly, silencing of MTH1 in AB1 mesothelioma tumors rendered them unresponsive to the regimen. Collectively, the aforementioned results imply that intrinsic MTH1 levels of the tumor could predict its response to MTH1 inhibitors. The possibility that tumor MTH1 expression can be used as a biomarker predictive of response to TH1579 or other similar agents requires further clinical evaluation.

Apart from the established effects of MTH1 inhibition on tumor cell survival, this study is the first to our knowledge to outline its antiangiogenic properties. Noteworthy, we show that these effects

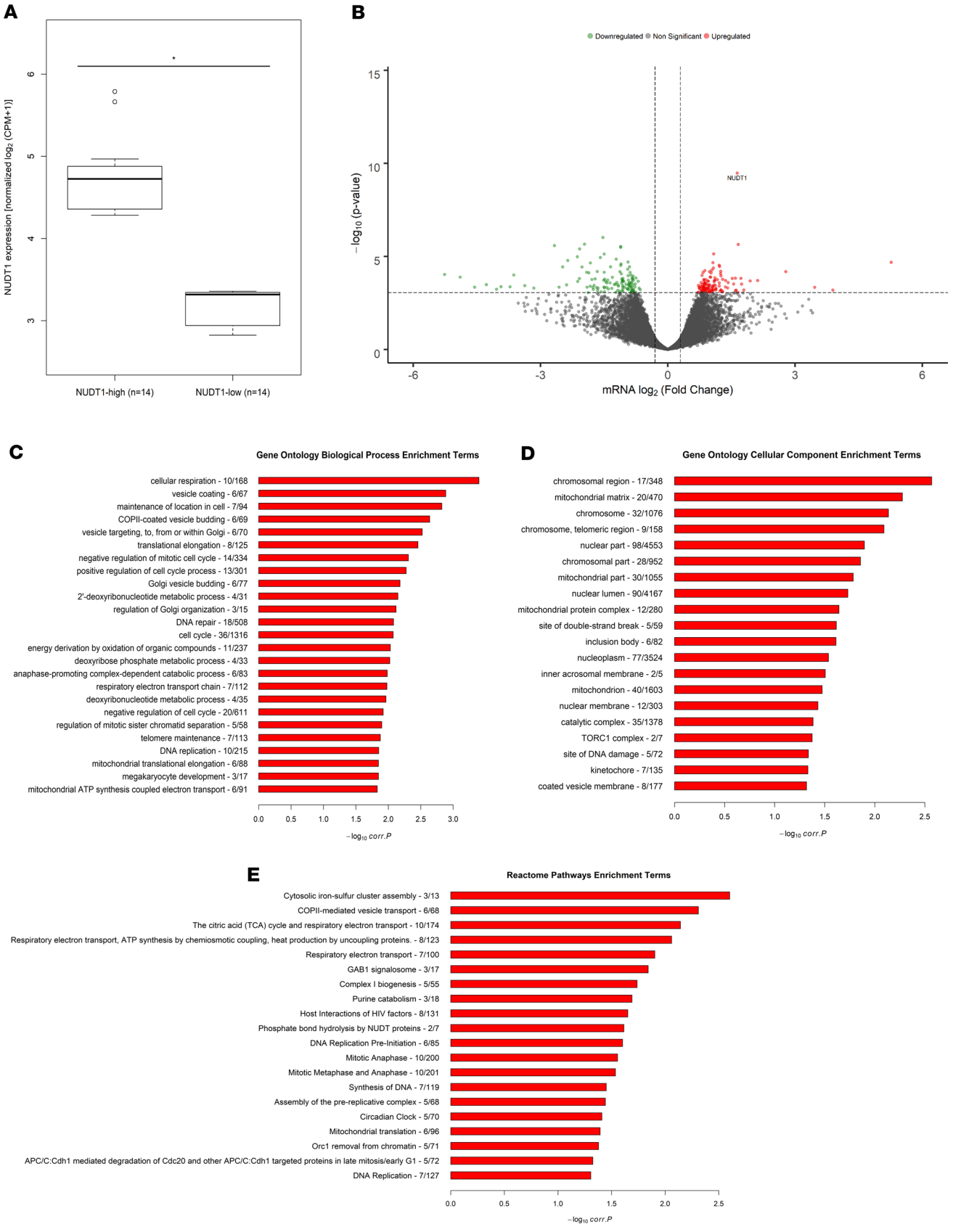
A
NUDT1 expression [normalized log2 (CPM+1)]
NUDT1-high (n=14)
NUDT1-low (n=14)
B
Downregulated Non Significant Upregulated
−log10 (p-value)
NUDT1
mRNA log2 (Fold Change)
C
Gene Ontology Biological Process Enrichment Terms
cellular respiration - 10/168
vesicle coating - 6/67
maintenance of location in cell - 7/94
COPII-coated vesicle budding - 6/69
vesicle targeting, to, from or within Golgi - 6/70
translational elongation - 8/125
negative regulation of mitotic cell cycle - 14/334
positive regulation of cell cycle process - 13/301
Golgi vesicle budding - 6/77
2'-deoxyribonucleotide metabolic process - 4/31
regulation of Golgi organization - 3/15
DNA repair - 18/508
cell cycle - 36/1316
energy derivation by oxidation of organic compounds - 11/237
deoxyribose phosphate metabolic process - 4/33
anaphase-promoting complex-dependent catabolic process - 6/83
respiratory electron transport chain - 7/112
deoxyribonucleotide metabolic process - 4/35
negative regulation of cell cycle - 20/611
regulation of mitotic sister chromatid separation - 5/58
telomere maintenance - 7/113
DNA replication - 10/215
mitochondrial translational elongation - 6/88
megakaryocyte development - 3/17
mitochondrial ATP synthesis coupled electron transport - 6/91
−log10 corr.P
D
Gene Ontology Cellular Component Enrichment Terms
chromosomal region - 17/348
mitochondrial matrix - 20/470
chromosome - 32/1076
chromosome, telomeric region - 9/158
nuclear part - 98/4553
chromosomal part - 28/952
mitochondrial part - 30/1055
nuclear lumen - 90/4167
mitochondrial protein complex - 12/280
site of double-strand break - 5/59
inclusion body - 6/82
nucleoplasm - 77/3524
inner acrosomal membrane - 2/5
mitochondrion - 40/1603
nuclear membrane - 12/303
catalytic complex - 35/1378
TORC1 complex - 2/7
site of DNA damage - 5/72
kinetochore - 7/135
coated vesicle membrane - 8/177
−log10 corr.P
E
Reactome Pathways Enrichment Terms
Cytosolic iron-sulfur cluster assembly - 3/13
COPII-mediated vesicle transport - 6/68
The citric acid (TCA) cycle and respiratory electron transport - 10/174
Respiratory electron transport, ATP synthesis by chemiosmotic coupling, heat production by uncoupling proteins. - 8/123
Respiratory electron transport - 7/100
GAB1 signalosome - 3/17
Complex I biogenesis - 5/55
Purine catabolism - 3/18
Host Interactions of HIV factors - 8/131
Phosphate bond hydrolysis by NUDT proteins - 2/7
DNA Replication Pre-Initiation - 6/85
Mitotic Anaphase - 10/200
Mitotic Metaphase and Anaphase - 10/201
Synthesis of DNA - 7/119
Assembly of the pre-replicative complex - 5/68
Circadian Clock - 5/70
Mitochondrial translation - 6/96
Orc1 removal from chromatin - 5/71
APC/C:Cdh1 mediated degradation of Cdc20 and other APC/C:Cdh1 targeted proteins in late mitosis/early G1 - 5/72
DNA Replication - 7/127
−log10 corr.P

Figure 6. Computational enrichment analysis significantly associates differentially expressed genes in high versus low *MTH1* human mesothelioma patients with functionally relevant biological processes, cellular components, and pathways. (**A**) Tukey-style box plots depicting *MTH1* (*NUDT1*) TMM normalized expression levels of the selected high- and low-expressing patients groups in $\log_2$ scale. Mann-Whitney-Wilcoxon statistical significance test for 2-group comparison ($P = 4.985 \times 10^{-8}$) *NUDT1*-high ($n = 14$) (lower whisker, 4.28; lower hinge, 4.36; median, 4.73; upper hinge, 4.88; upper whisker, 4.97; outliers, 5.66 and 5.79) *NUDT1*-low ($n = 14$) (lower whisker, 2.82; lower hinge, 2.94; median, 3.32; upper hinge, 3.35; upper whisker, 3.36). (**B**) Volcano plot of upregulated (red) and downregulated (green) DEGs between groups of high and low *MTH1* expression. Horizontal dashed line represents the highest *P* value in negative $\log_{10}$ scale that corresponds to an adjusted $P < 0.05$. Vertical dashed lines correspond to $|\log_2(\text{fold change})| > 0.3$ threshold. Gray dots mark nonstatistically significant altered genes. (**C**) Gene Ontology enrichment analysis for significantly related GO terms of biological processes. Chart presents the top 25 among 78 in total GO terms (Supplemental Table 2). (**D**) GO enrichment analysis for significantly associated GO terms of cellular components (Supplemental Table 3). (**E**) Reactome Pathway enrichment analysis (Supplemental Table 4). *y* axis, term and gene enrichment; *x* axis, corrected *P* value in negative $\log_{10}$ scale.

are restricted to tumor endothelium. TECs express higher levels of MTH1 than normal ones and are, therefore, more vulnerable to pharmacological targeting of the enzyme. This finding could be attributed to elevated intracellular ROS levels of TECs compared with normal ones (12). MTH1 inhibitors may therefore exert a dual role, affecting both tumor progression and its supporting vasculature. Additionally, since they preferably target tumor endothelium without affecting normal vessels, they are expected to overcome the increased toxicity issues raised by current antiangiogenic regimens. Most importantly, MTH1 inhibitors are likely to surpass the emergence of adaptive resistance due to the fact that they target the cell cycle checkpoint of endothelial cells rather than specific angiogenic mediators, which is the case of currently used inhibitors of tumor angiogenesis. In fact, current antiangiogenic therapies sooner or later confer the compensatory activation of alternative angiogenic pathways (25) and vessel cooption (26). Another important and potentially novel observation of the present study is the relation between tumoral and endothelial MTH1 levels. MTH1-overexpressing tumors have the capacity to manipulate endothelial functions by elevating MTH1 expression in them, favoring their survival and promoting their own spread and vascularization. To explain this, we propose a model where DNA secreted by tumor cells is detected by endothelial cells and regulates their MTH1 levels and subsequent survival through TLR9-mediated NF-κB signaling. This finding adds to emerging recent evidence on the role of secreted and cytosolic DNA in tumor progression and metastasis (27, 28). In our hands, signaling is dependent on different amounts of 8-Oxo-dG of the secreted DNA that is sensored by tumor endothelium. In fact, endothelial cells are known to upregulate their ROS and NO production upon treatment with oxidized extracellular DNA (rich in 8-Oxo-dG) in vitro (29). We demonstrate that treatment of TECs with the more oxidized DNA upregulated NF-κB and attenuated their survival. Indeed, unlike tumor cells, it has been shown that inhibition of NF-κB activation in endothelial cells promotes angiogenesis in vivo (30, 31). We therefore assume that mesothelioma tumor cells may precondition the bystander endothelium, enhancing its resistance to oxidative stress, and may promote angiogenesis for their own benefit. Our evidence suggests that triggering of the angiogenic process is (at least partially) mediated through the TLR9/NF-κB/MTH1 axis in endothelial cells. In accordance with our results, TLR9/NF-κB triggering resulted in revascularization and regrowth of murine tumors upon irradiation-induced DNA damage (32).

The proposed mechanistic model derived from our in vivo and in vitro experiments is compatible with the presented computational analysis of available RNA-seq data from human mesotheliomas. It was found that high- versus low *MTH1*–expressing mesothelioma tumors were significantly differentiated in terms of several systems processes, components, and pathways, which overall fall into 3 major biological categories: DNA repair, cell cycle/mitosis, and microvesicle trafficking. Although the role of MTH1 in the 2 first pivotal cellular functions is well documented (3, 6, 7), this is the first study to our knowledge connecting MTH1 expression with the secretory machinery. While this finding cannot explain the exact mechanisms connecting MTH1 and microvesicle signaling, it argues toward the importance of them during oxidative stress and enhanced DNA repair conditions. In fact, emerging data document an increase of microvesicle excretion upon DNA damaging agents and outline their role in the homeostatic sanitization of the producing cell (33–35). In relation to this, DNA damage repair and the secretory machinery (ER stress) are known to be intertwined, to crosstalk, and to share common regulators (such as ATFs, NF-κB) and check points (i.e., H2Ax) (36). Finally, the functional analysis of RNA-seq mesothelioma data also unveiled an implication of MTH1 expression with the angiogenic process. This result corroborates with emerging evidence attributing proangiogenic potencies at several DNA damage and repair genes (12, 23, 37–40).

In conclusion, the studies presented here underline the importance of MTH1 targeting in limiting mesothelioma progression and mesothelioma-associated pleural fluid accumulation and provide a rationale for further clinical testing. What makes MTH1 an appealing target for mesothelioma treatment is that (a) its tumoral levels are associated with patients survival, (b) it is not an oncogene, (c) it is a synthetic lethal for both mesothelioma cells and supporting endothelium, and d) it mediates a signal transduction from the tumor cells toward bystander endothelial that favors survival and progression of both. Our findings could, thus, be clinically exploited for the development of more effective mesothelioma treatment.

Methods

Cell lines and reagents

AE17 and AB1 murine mesothelioma cell lines were generated by B. Robinson and provided by YCG Lee (Centre for Asthma, Allergy, and Respiratory Research, School of Medicine and Pharmacology, University of Western Australia, Perth, Western Australia). Human ZL34 and MSTO-211H mesothelioma cell lines were purchased from MilliporeSigma. All cell lines were maintained in DMEM (10% FBS). AE17 cells overexpressing MTH1 were created upon stable transfection with *Nudt1* (NM_008637) ORF clone (Origene Technologies Inc.). AB1 cells of silenced MTH1 expression (AB1shmth1) were created upon stable transfection with *Nudt1* mouse shRNA plasmid (Locus ID 17766; TL501390, Origene Technologies Inc.). In both cases, MTH1 overexpression or silencing was verified by Western blot, and potential alterations in their cell viability were evaluated by XTT (XTT Cell viability assay kit, Biotium Inc.). Murine endothelial cells of normal lungs (NECs) or TECs were released from naive lungs, adjacent normal lung, or mesothelioma tumors, as previously described (41).

MTH1 inhibitor (Karolinska Nudt1 inhibitor, Karonudib, or TH1579) was developed (designed and synthesized) and provided by Thomas Helleday (Division of Translational Medicine and Chemical Biology Karolinska Institutet, SciLifeLab). TH1579 was freshly prepared and formulated with hydroxypropyl-β-cyclodextrin (HPβCD, 10% w/v) (AppliChem GmbH) in acetate buffer (pH 4.5). N-acetyl-cysteine (NAC) was purchased from Tocris. Murine TNF-α and BAY1170-82 were purchased from PeproTech. Phorbol myristate acetate (PMA) was obtained from Merck.

In vivo studies

C57BL/6 and BALB/c mice were purchased from BSRC Alexander Fleming, and NOD.CB17-Prkdcscid/J (NOD.SCID) mice were obtained from Pasteur Institute. All strains were housed at the Animal Model Research Unit of Evangelismos Hospital, receiving food and water ad libitum.

Human xenografts. Eight- to 10-week-old NOD.SCID mice were s.c. injected with ZL34 or MSTO-211H cells (2×10^6 cells/mouse) in the right flank. Once tumors reached 200 mm^3, animals were split to 2 groups, receiving vehicle (10% HPβCD) or TH1579 (90 mg/kg body weight) 2 times per day, every 2 days, p.o. (oral gavage). Tumor volume was measured thrice weekly and was calculated using the formula $V = (\text{length} \times \text{width}^2)/2$. Mice were euthanized 24–27 days upon initiation of the experiment, tumors were excised and weighed, and samples were stored for subsequent analysis.

Syngeneic models. AE17 or AB1 (5×10^5) mesothelioma cells were intrapleurally injected in 8- to 10-week-old C57BL/6 or BALB/c syngeneic mice, respectively (42). Four days upon tumor cell implantation, animals were divided into 2 groups, receiving either TH1579 or vehicle as mentioned previously. In order to investigate the role of MTH1 expression levels in mesothelioma tumor growth and response to the inhibitor, AB1 vector or AB1shmth1 and AE17 vector or AE17 MTH1–overexpressing cells were injected in syngeneic mice and were subsequently split to 4 groups, receiving vehicle or TH1579, as mentioned previously.

In all cases, animals were euthanized 12–14 days after pleural delivery of tumor cells. Pleural fluid, tumors, lungs, and blood were collected and stored for subsequent analysis. Mesothelioma tumors were collected and weighed, while pleural fluid was retrieved and quantified.

In vitro studies

IHC and immunofluorescence. Formalin-fixed paraffin tumor tissue sections were immunohistochemically analyzed for PCNA (1:1000, D3H8P, Cell Signaling Technology) for evaluation of tumor cell proliferation. Tumor cell apoptosis was assessed by TUNEL (42). For immunofluorescence analysis, tumor cryosections were stained for the presence of CD31 (1:50, clone MEC 13.3, BD Biosciences) and

caspase-3 (1:50, 9669, Cell Signaling Technology) for endothelial and apoptotic cell staining, respectively. Colocalization analysis of caspase-3 and CD31 was performed by ImageJ software (NIH). For 8-Oxo-dG and γH2AX quantification, anti–8-Oxo-dG (1:100, MAB3560, MilliporeSigma) and γH2AX (05-636, MilliporeSigma) were employed.

Real-time PCR

Quantification of *Mth1* mRNA expression levels was performed by real-time PCR. Total mRNA of AB1, AE17, AE17 vector, and AE17 MTH1overexpressing cells — as well as TECs and NECs — were isolated by Nucleospin RNAplus kit (Macherey-Nagel). cDNA was prepared using the PrimeScript 1st strand cDNA Synthesis kit (Takara, Clontech). *Mth1* mRNA levels were evaluated in reference to *Gapdh* expression, as described previously (3).

Cell viability

NECs and TECs were seeded at 6×10^3 cells/well in 96-well plates. In all cases, media were removed 24 hours later and replaced with fresh complete medium containing vehicle or escalating doses of TH1579 (1–1000 μM). Cell viability was subsequently measured by XTT reduction at 450 nm (XTT Cell viability assay kit, Biotium Inc.).

Migration

TECs and NECs isolated as mentioned previously were seeded onto 6-well plates and left overnight. Cells were subsequently serum starved for 4 hours and loaded onto Transwell upper compartments (Corning Costar Transwell cell culture inserts, CLS3464-48EA, Merck) at a density of 6×10^4 cells/100 μL in the presence of 10 nM TH1579 or vehicle. Cells were left to migrate toward full medium for 16 hours. Migrated cells were fixed, stained by tolouidine blue, and counted under a microscope.

Tube formation

TECs and NECs isolated as mentioned previously were seeded onto 24-well plates precoated with Matrigel (Geltrex-LDEV, A1413201, Thermo Fisher Scientific) at a density of 6×10^4 cells/well in serum-free medium containing 10 nM TH1579 or vehicle. Endothelial cells were left to form tube-like networks overnight. Resulting EC networks were fixed and photographed under a microscope, and total length was determined using ImageJ software using the vessel length plugin application available (NIH).

Western blotting

TECs were seeded onto 6-well plates at a density of 2×10^5 cells/well and serum starved overnight. cfDNA secreted by AE17, AE17 MTH1–overexpressing cells, or AE17 cells treated with NAC (5 mM, overnight) isolated from culture supernatants using a commercial kit (Nucleospin, Macherey-Nagel). TECs were subsequently treated with 20 ng/mL extracellular DNA of the aforementioned conditions and/or TNF-α (20 ng/mL), PMA (5 mM), and BAY1170-82 (10 μM) for 2–18 hours. TLR9 inhibitor chloroquine (Merck) was used at 2 μg/mL 40 minutes before addition of cfDNA. Cell lysates were prepared and analyzed by Western blotting for phospho-p65 NF-κB (Cell Signaling Technology, 3031), total p65 NF-κB (Cell Signaling Technology, 4764), and MTH1 (Origene Technologies Inc., 332710). Results were normalized to actin and quantified using GelPro Analyzer (Media Cybernetics)

ChIP assay

ChIP assay was preformed using the Chromatin Immunoprecipitation assay kit (MilliporeSigma). In brief, TECs from mesothelioma AE17 tumors were isolated as mentioned previously. Confluent cultures (Petri dishes to obtain more than 1×10^6 cells) were serum starved overnight and subsequently treated with vehicle (PBS) or cfDNA from AE17, AE17 MTH1–overexpressing cells, or AE17 cells treated with NAC (5mM, overnight) (20 ng/mL). TNF-α (20 ng/mL) was used as a positive control (NF-κB activator). Cells were collected 18 hours later, histones were cross-linked to DNA using formaldehyde (1%), and DNA-protein complexes were sheared. DNA fragments associated with NF-κB were precipitated using an anti–NF-κB antibody (1/100, D14E12, Cell signaling Technology). A negative control (NC, no antibody) was also included. DNA fragments associated with NF-κB were eluted and *Mth1* sequence was detected by real-time PCR.

Fragment size evaluation of cfDNA samples

The size of cfDNA isolated by AE17 cell culture supernatants was analyzed using capillary electrophoresis (CE) at an Agilent 2100 Bioanalyzer (Agilent Technologies Inc.) and a High Sensitivity DNA kit (Agilent Technologies Inc.). Analysis was performed by an Agilent 2100 Expert Software that calculates the sizes of DNA fragments, and results are presented as an electropherogram.

8-Oxo-dG quantification

DNA secreted in cell supernatants of AE17, AE17 MTH1–overexpressing cells, or AE17 cells treated with NAC (5 mM, overnight) was isolated using a commercial kit (Nucleospin, Macherey-Nagel), and levels of oxidized Guanosine (8-Dihydro-8-Oxo-2'-Deoxyguanosine) were quantified using ELISA according to manufacture instructions (RDR-8-OHdG-Ge, Reddot Biotech). Results were normalized to total nanograms of DNA loaded for the assays determined in a NanoDrop device (Thermo Fisher Scientific).

Human mesothelioma RNA-seq data analysis

Mesothelioma gene-level raw expression RNA-seq data produced by RSEM software (43) (MESO.uncv2.mRNAseq_raw_counts.txt), along with clinical information, were downloaded from Broad Institute TCGA Genome Data Analysis Center Firehose (https://gdac.broadinstitute.org/) (44). The results presented here are, in whole, based upon data generated by the TCGA Research Network (https://www.cancer.gov/tcga; accessed in December 2018).

Bioinformatic analysis of TCGA data

Survival curve. Survival analysis of mesothelioma patients based on their *NUDT1* mRNA expression levels was performed using UALCAN interactive portal (http://ualcan.path.uab.edu/analysis.html) (45).

Identification of DEGs and functional annotation. Out of the total 87 mesothelioma patients, 57 available epithelioid histological subtype cases were stratified based on *NUDT1* expression (counts per million, CPM), after Trimmed Mean of M-values (TMM) normalization (46). Remaining sarcomatoid, biphasic, and mixed subtype samples were excluded, in order to reduce tumor heterogeneity and focus on *NUDT1* expression–associated traits. The *NUDT1*-high group included patients with *NUDT1* expression above the 75% percentile, while the *NUDT1*-low group included patients below the 25% percentile. Statistical significance of *NUDT1* expression difference between the aforementioned groups was assessed by Mann-Whitney-Wilcoxon nonparametric test. Between-group differential expression analysis was conducted using the edgeR package in R (47, 48). The glmTreat function of edgeR was implemented for testing significant differences relative to fold-change thresholds. Genes with an adjusted P value (Benjamini–Hochberg multiple hypothesis testing correction for FDR control) < 0.05 and $|\log_2(\text{fold change})| > 0.3$ were considered as differentially expressed. The volcano plot illustrating identified DEGs was created using the EnhancedVolcano package in R (49). Subsequent GO and Reactome Pathway enrichment analysis was performed using the Bioinfominer software (50, 51), a tool for intelligent, automated interpretation of genomic data. A significance threshold of corrected $P < 0.05$ was adopted for altered biological terms.

Statistics

All values are presented as mean ± SEM. Differences between groups were evaluated using the 2-tailed Student's t test or 1-way ANOVA with Bonferroni's post hoc test for multiple comparisons, as appropriate. $P < 0.05$ were considered significant. Statistical analysis was performed using the Statistical Package for the Social Sciences v.13.0.0 (IMB).

Study approval

Experiments were approved by the Veterinary Administration Bureau, Prefecture of Athens, Greece (decision no: 1343, 03/03/2016 and 117264, 11/02/2020) under compliance to the national law and the EU Directives.

Author contributions

SFM, PCV, AGP, PCA, ISP, CAM, MPI, and CNK performed experiments; SFM and ITK contributed conception and design; SFM, PCV, AGP, PCA, ISP, CAM, MPI, CNK, HVL, VGG, and ITK analyzed and interpreted data; and SFM, HVL, VGG, and ITK drafted the manuscript for intellectual content.

Acknowledgments

We acknowledge Ulrika Warpman Berglund and Thomas Helleday (Karolinska Instituet, Solna, Sweden) for valuable scientific discussions and provision of TH1579. Authors thank Giannis Vatsellas (BRFAA, Athens, Greece) for his valued technical support. We also thank E. Aravidou and Z. Kollia (Research Unit for animal standards, Evangelismos Hospital, Athens, Greece) for professional veterinarian and animal care assistance, respectively. This work was supported by a grant from the Hellenic Thoracic Society. We thank the National and Kapodistrirtian University of Athens for funding the publication of the present paper.

Address correspondence to: Sophia Magkouta, Marianthi Simou Lab, 3 Ploutarchou st, 2nd Floor, 10675, Athens, Greece. Phone: 30.210.72.35.521; Email: smagkouta@med.uoa.gr.

1. Zhang Y, Du Y, Le W, Wang K, Kieffer N, Zhang J. Redox control of the survival of healthy and diseased cells. *Antioxid Redox Signal*. 2011;15(11):2867–2908.
2. Luo M, He H, Kelley MR, Georgiadis MM. Redox regulation of DNA repair: implications for human health and cancer therapeutic development. *Antioxid Redox Signal*. 2010;12(11):1247–1269.
3. Gad H, et al. MTH1 inhibition eradicates cancer by preventing sanitation of the dNTP pool. *Nature*. 2014;508(7495):215–221.
4. Patel A, et al. MutT Homolog 1 (MTH1) maintains multiple KRAS-driven pro-malignant pathways. *Oncogene*. 2015;34(20):2586–2596.
5. Tu Y, et al. Birth of MTH1 as a therapeutic target for glioblastoma: MTH1 is indispensable for gliomatumorigenesis. *Am J Transl Res*. 2016;8(6):2803–2811.
6. Warpman Berglund U, et al. Validation and development of MTH1 inhibitors for treatment of cancer. *Ann Oncol*. 2016;27(12):2275–2283.
7. Einarsdottir BO, et al. A patient-derived xenograft pre-clinical trial reveals treatment responses and a resistance mechanism to karonudib in metastatic melanoma. *Cell Death Dis*. 2018;9(8):810.
8. van der Waals LM, Laoukili J, Jongen JMJ, Raats DA, Borel Rinkes IHM, Kranenburg O. Differential anti-tumour effects of MTH1 inhibitors in patient-derived 3D colorectal cancer cultures. *Sci Rep*. 2019;9(1):819.
9. Le Stang N, et al. Incidence and survival of peritoneal malignant mesothelioma between 1989 and 2015: A population-based study. *Cancer Epidemiol*. 2019;60:106–111.
10. Baas P, et al. Malignant pleural mesothelioma: ESMO Clinical Practice Guidelines for diagnosis, treatment and follow-up. *Ann Oncol*. 2015;26 Suppl 5:v31–v39.
11. Benedetti S, Nuvoli B, Catalani S, Galati R. Reactive oxygen species a double-edged sword for mesothelioma. *Oncotarget*. 2015;6(19):16848–16865.
12. Okuno Y, Nakamura-Ishizu A, Otsu K, Suda T, Kubota Y. Pathological neoangiogenesis depends on oxidative stress regulation by ATM. *Nat Med*. 2012;18(8):1208–1216.
13. Hojo T, et al. ROS enhance angiogenic properties via regulation of NRF2 in tumor endothelial cells. *Oncotarget*. 2017;8(28):45484–45495.
14. Wilson R, et al. MicroRNA regulation of endothelial TREX1 reprograms the tumour microenvironment. *Nat Commun*. 2016;7:13597.
15. Gorgoulis VG, Pefani DE, Pateras IS, Trougakos IP. Integrating the DNA damage and protein stress responses during cancer development and treatment. *J Pathol*. 2018;246(1):12–40.
16. Bronkhorst AJ, Wentzel JF, Aucamp J, van Dyk E, du Plessis L, Pretorius PJ. Characterization of the cell-free DNA released by cultured cancer cells. *Biochim Biophys Acta*. 2016;1863(1):157–165.
17. Mathieu M, Martin-Jaular L, Lavieu G, Théry C. Specificities of secretion and uptake of exosomes and other extracellular vesicles for cell-to-cell communication. *Nat Cell Biol*. 2019;21(1):9–17.
18. Wang W, et al. Characterization of the release and biological significance of cell-free DNA from breast cancer cell lines. *Oncotarget*. 2017;8(26):43180–43191.
19. Aucamp J, Bronkhorst AJ, Badenhorst CPS, Pretorius PJ. The diverse origins of circulating cell-free DNA in the human body: a critical re-evaluation of the literature. *Biol Rev Camb Philos Soc*. 2018;93(3):1649–1683.
20. Reuven EM, Fink A, Shai Y. Regulation of innate immune responses by transmembrane interactions: lessons from the TLR family. *Biochim Biophys Acta*. 2014;1838(6):1586–1593.
21. Bobrovnikova-Marjon E, et al. PERK promotes cancer cell proliferation and tumor growth by limiting oxidative DNA damage. *Oncogene*. 2010;29(27):3881–3895.
22. Schmitz ML, Shaban MS, Albert BV, Gökçen A, Kracht M. The Crosstalk of Endoplasmic Reticulum (ER) Stress Pathways with NF-κB: Complex Mechanisms Relevant for Cancer, Inflammation and Infection. *Biomedicines*. 2018;6(2):E58.
23. Yamamori T, Meike S, Nagane M, Yasui H, Inanami O. ER stress suppresses DNA double-strand break repair and sensitizes tumor cells to ionizing radiation by stimulating proteasomal degradation of Rad51. *FEBS Lett*. 2013;587(20):3348–3353.
24. Hua X, et al. Karonudib is a promising anticancer therapy in hepatocellular carcinoma. *Ther Adv Med Oncol*. 2019;11:1758835919866960.
25. Bergers G, Hanahan D. Modes of resistance to anti-angiogenic therapy. *Nat Rev Cancer*. 2008;8(8):592–603.
26. Voutouri C, et al. Experimental and computational analyses reveal dynamics of tumor vessel cooption and optimal treatment strategies. *Proc Natl Acad Sci USA*. 2019;116(7):2662–2671.
27. Bakhoum SF, et al. Chromosomal instability drives metastasis through a cytosolic DNA response. *Nature*. 2018;553(7689):467–472.
28. Wortzel I, Dror S, Kenific CM, Lyden D. Exosome-Mediated Metastasis: Communication from a Distance. *Dev Cell*. 2019;49(3):347–360.

29. Kostyuk SV, et al. Role of extracellular DNA oxidative modification in radiation induced bystander effects in human endotheliocytes. *Mutat Res*. 2012;729(1-2):52–60.
30. Kisseleva T, Song L, Vorontchikhina M, Feirt N, Kitajewski J, Schindler C. NF-kappaB regulation of endothelial cell function during LPS-induced toxemia and cancer. *J Clin Invest*. 2006;116(11):2955–2963.
31. Tabruyn SP, et al. NF-kappaB activation in endothelial cells is critical for the activity of angiostatic agents. *Mol Cancer Ther*. 2009;8(9):2645–2654.
32. Gao C, et al. TLR9 signaling in the tumor microenvironment initiates cancer recurrence after radiotherapy. *Cancer Res*. 2013;73(24):7211–7221.
33. Takahashi A, et al. Exosomes maintain cellular homeostasis by excreting harmful DNA from cells. *Nat Commun*. 2017;8:15287.
34. Lian Q, et al. Chemotherapy-induced intestinal inflammatory responses are mediated by exosome secretion of double-strand DNA via AIM2 inflammasome activation. *Cell Res*. 2017;27(6):784–800.
35. Takasugi M, Okada R, Takahashi A, Virya Chen D, Watanabe S, Hara E. Small extracellular vesicles secreted from senescent cells promote cancer cell proliferation through EphA2. *Nat Commun*. 2017;8:15729.
36. Dicks N, Gutierrez K, Michalak M, Bordignon V, Agellon LB. Endoplasmic reticulum stress, genome damage, and cancer. *Front Oncol*. 2015;5:11.
37. Economopoulou M, et al. Histone H2AX is integral to hypoxia-driven neovascularization. *Nat Med*. 2009;15(5):553–558.
38. Dong D, et al. Critical role of the stress chaperone GRP78/BiP in tumor proliferation, survival, and tumor angiogenesis in transgene-induced mammary tumor development. *Cancer Res*. 2008;68(2):498–505.
39. Virrey JJ, et al. Stress chaperone GRP78/BiP confers chemoresistance to tumor-associated endothelial cells. *Mol Cancer Res*. 2008;6(8):1268–1275.
40. Katanasaka Y, et al. Cancer antineovascular therapy with liposome drug delivery systems targeted to BiP/GRP78. *Int J Cancer*. 2010;127(11):2685–2698.
41. Wang J, Niu N, Xu S, Jin ZG. A simple protocol for isolating mouse lung endothelial cells. *Sci Rep*. 2019;9(1):1458.
42. Pappas AG, et al. Versican modulates tumor-associated macrophage properties to stimulate mesothelioma growth. *Oncoimmunology*. 2019;8(2):e1537427.
43. Li B, Dewey CN. RSEM: accurate transcript quantification from RNA-Seq data with or without a reference genome. *BMC Bioinformatics*. 2011;12:323.
44. Broad Institute TCGA Genome Data Analysis Center. Analysis-ready standardized TCGA data from Broad GDAC Firehose 2016_01_28 run. Broad Institute of MIT and Harvard. https://doi.org/10.7908/C11G0KM9. Accessed June 1, 2020.
45. Chandrashekar DS, et al. UALCAN: A Portal for Facilitating Tumor Subgroup Gene Expression and Survival Analyses. *Neoplasia*. 2017;19(8):649–658.
46. Robinson MD, Oshlack A. A scaling normalization method for differential expression analysis of RNA-seq data. *Genome Biol*. 2010;11(3):R25.
47. Robinson MD, McCarthy DJ, Smyth GK. edgeR: a Bioconductor package for differential expression analysis of digital gene expression data. *Bioinformatics*. 2010;26(1):139–140.
48. McCarthy DJ, Chen Y, Smyth GK. Differential expression analysis of multifactor RNA-Seq experiments with respect to biological variation. *Nucleic Acids Res*. 2012;40(10):4288–4297.
49. Blighe K. EnhancedVolcano: Publication-ready volcano plots with enhanced coloring and labeling. Package version 1.0.1. https://github.com/kevinblighe/EnhancedVolcano. Accessed June 9, 2020.
50. Koutsandreas T, Binenbaum I, Valavanis I, Papadodima O, Chantziioannou A. Analyzing and Visualizing Genomic Complexity for the Derivation of the Emergent Molecular Networks. *Int J Monit Surveill Technol Res*. 2016;4(2).
51. Lhomond S, et al. Dual IRE1 RNase functions dictate glioblastoma development. *EMBO Mol Med*. 2018;10(3):e7929.